Polymer-like to Soft Colloid-like Behavior of Regular Star Polymers Adsorbed on Surfaces

Emmanouil Glynos,[†] Alexandros Chremos,[‡] George Petekidis,[§,#] Philip J. Camp,[‡] and Vasileios Koutsos*[,†]

Institute for Materials and Processes, School of Engineering and Electronics & Centre for Materials Science and Engineering, University of Edinburgh, King's Buildings, Edinburgh EH9 3JL, United Kingdom; School of Chemistry, University of Edinburgh, West Mains Road, Edinburgh EH9 3JJ, United Kingdom; Institute of Electronic Structure and Laser-FORTH, PO Box 1527, Heraklion 71110, Crete, Greece; and Department of Materials Science and Technology, University of Crete, Heraklion, Crete, Greece

Received April 14, 2007; Revised Manuscript Received June 15, 2007

ABSTRACT: We investigated systematically the structure and growth of monolayers of physisorbed polybutadiene (PB) starlike polymers on freshly cleaved mica after solvent evaporation using atomic force microscopy (AFM). We observed a strong dependence of the evolution of the average island height and surface coverage with increasing surface density on the functionality (number of arms) of the star polymers. We explain these structural phenomena in terms of the molecular and conformational properties of the different star polymers. Our study provides real space observations of the star polymer surface structures near the overlap surface density for the first time. The structural regimes are strongly affected by the change of the star polymer behavior from polymer-like to colloid-like when the arm functionality increases.

Introduction

Polymers on surfaces play an important role for many technological applications such as microelectronics, colloidal stability,[1,2] surface nanopatterning,[3] adhesion,[4] and friction modification.[5,6] Linear polymers on surfaces have been extensively studied experimentally.[7−13] Although several recent studies focused on heteroarm star copolymers,[14−19] the rather simpler case of star homopolymers adsorbed on surfaces has largely been ignored.

Recent advances in polymer chemistry led to the synthesis of a wide range of new materials, such as star-shaped macromolecules with large numbers of homopolymer arms covalently joined to a dendritic core. Star polymers can be considered molecules with intermediate character between colloids and polymers;[20] thus, they represent a soft matter system bridging two very important scientific fields with long histories and important industrial applications. The intermediate behavior of star polymers renders them ideal for the design of novel systems and materials with fine-tuned intermediate physical properties. Thus, star polymers have attracted considerable interest during the past few years, and several studies have already been reviewed.[21,22] These reviews focused on experiments, theory, and simulations of star polymer systems mainly away from surfaces. From the experimental point of view, the fact that star polymers, which are nearly monodisperse in both the number of arms and the degree of polymerization, can be synthesized by anionic polymerization by chemists[23,24] has played an important role in the development of the field since it made possible the exploration of well-defined model systems.

The conformation of an isolated star was meticulously explained by Daoud and Cotton, using scaling theory to introduce the blob model of a star polymer.[25] In this model the star polymer was considered as a succession of concentric shells of blobs, the sizes of which, $\xi(r)$, depend on the distances of the blob from the center of the star leading to a nonuniform monomer density distribution, $c(r)$, which has been verified experimentally and by computer simulations.[22] The nonuniform monomer density distribution results in a nonuniform osmotic pressure of the star which decreases from its maximum at the center (core) to the outer part (corona) of the star polymer. Star polymers can be considered as molecular entities with two characteristic length scales: a small one of polymeric nature corresponding to interacting blobs (self-avoiding segments) and a large one of colloidal nature which corresponds to its overall size.

A lot of studies have focused on star polymer dynamics, and results have already been reviewed by Vlassopoulos et al.[26] The generic behavior of the star is described in terms of the competition between its polymeric and colloidal characters which strongly depends on the functionality, f (number of arms), of the star. More specifically, they showed experimentally that the interpenetration between stars increases with decreasing f. This stems from the fact that the osmotic pressure within the star increases with the star polymer functionality, preventing interpenetrations between different star polymers. Studies on the concentration dependence of the viscosity of star polybutadiene solutions (systems similar to the one studied in this work) showed molecular, tunable softness from entangled polymers ($f < 32$) to soft colloidal spheres ($f > 32$).[22,26] The softness of the star with respect to f has also been studied comprehensively by Likos et al.[27] using fluid-state theory and Monte Carlo simulations. By calculating the star−star interactions for arbitrary distance, r, between their cores, they showed that the softness of a star polymer decreases with increasing f. Hence, low functionality leads to low osmotic pressure of the star polymer, which in turn makes the star polymer softer.

* To whom correspondence should be addressed. E-mail: vasileios.koutsos@ed.ac.uk.
[†] School of Engineering and Electronics & Centre for Materials Science and Engineering, University of Edinburgh.
[‡] School of Chemistry, University of Edinburgh.
[§] Institute of Electronic Structure and Laser-FORTH.
[#] Department of Materials Science and Technology, University of Crete.

10.1021/ma0708803 CCC: $37.00
Published on Web 08/21/2007

Table 1. Star Polybutadiene Molecular Characteristics

code	f	M_w (g/mol)	M_w^{arm} (g/mol)	R_g (nm)[a]	R_h (nm)[b]	R_b (nm)[c]	c^* (g/g)	$V_{molecule}$[d] (nm^3)
1518	18	311K	17K	12.4	15.4	5.17	0.073	580
3216	32	558K	17K	13.4	17.2	6.29	0.103	1040
6480	59	4200K	71K	34.1	47.7	12.32	0.047	7840

[a] Radius of gyration in dilute good solvent conditions from light scattering measurements.[26,35] [b] Hydrodynamic radius in dilute good solvent solutions.[26] [c] Calculated radius in bad-solvent conditions (compact sphere) using the bulk PB density value,[35] $\rho = 0.89$ g/cm^3. [d] Calculated volume of a collapsed molecule (based on the molecular weight and bulk density of PB).

An interesting line of investigation concerns the structural regimes and possible transitions of star solutions as one moves from the dilute regime of isolated stars to progressively dense structures as the concentration increases. Several structural regimes have been predicted by theory[28] and investigated experimentally[29,30] depending on the star functionality. In particular, simulations have predicted a fluid−crystal transition at a critical arm number of ∼34.[28] Nevertheless, although a liquid to glass transition has been observed experimentally around the overlap concentration for stars with f of ∼120,[29,30] a clear experimental observation of a crystal phase is still lacking. However, concentration-dependent structural studies have not been performed for star homopolymers adsorbed on surfaces. It has been predicted by simulations that a star with f arms near a surface adopts conformations very similar to those of an isolated star with $2f$ arms.[31] Thus, it is to be expected that the onset of the glass (or crystal) phase will be moved to lower critical arm numbers and concentrations for stars adsorbed on surfaces.

Theoretical[32] and simulation[33] studies showed that the polymer architecture plays an important role on its adsorption behavior. This is particularly relevant when the adsorption occurs in good solvent conditions since the polymer chains are swollen and entropic effects are dominant. Branched polymers can be adsorbed more easily because they have to pay a decreased entropic penalty compared to linear ones; however, linear chains can be adsorbed more strongly since they can spread and take flat conformations, maximizing their contact with the surface.[33]

AFM studies of star polymers adsorbed on surfaces have been so far restricted to the structure of isolated stars. Kiriy et al.[18] studied the structure of heteroarm star copolymers, polystyrene/poly(2-vinylpyridine) (PS−P2VP) with seven arms, adsorbed on mica and Si wafers by tapping mode AFM in air. They used dilute solutions of various good and selective solvents and rapid evaporation. They found that samples prepared from a good solvent resulted in globular conformations while those from selective solvents yielded extended surface conformations of one type of segments. In some cases, they used metal clusters permitting the enhanced AFM visualization of the few P2VP arm segments. An important conclusion of this work was that the history and treatment of samples had profound consequences on the polymer conformations on the surface. However, in several cases, mainly due to the rapid evaporation of the solvent, they claimed that the surface polymer structure resembled the structure of the polymer in the bulk solution.

In this paper, we investigate the structural regimes of submonolayers and monolayers of adsorbed PB star polymers of three different functionalities ($f = 18$, 32, and 59) on mica surfaces. The adsorption was attained by immersing the freshly cleaved mica surface into star solutions in toluene (good solvent for PB) at different concentrations well below the critical overlap concentration, c^*. An important aspect of our work is the pretreatment of the polymer-modified surfaces: extensive rinsing with toluene to remove any nonadsorbed molecules followed by an exposure in a pure toluene bath for several hours to attain as far as possible equilibrated conformations and finally a rapid solvent evaporation under flow of nitrogen. Imaging was performed using a tapping mode AFM in air. The resultant adsorbed structures were analyzed quantitatively and have provided direct information about the star behavior in bad solvent conditions (air). The observed dependence of the monolayer growth and structure on the star functionality and surface density have also yielded insight on the probable conformations and behavior of the adsorbed star polymers in good solvent conditions just before the evaporation of the solvent. Our study provides real space observations of the star polymer surface structures near the surface overlap density for the first time.

Experimental Section

Materials. A series of regular 1,4-polybutadiene multiarm stars were synthesized by Roovers and co-workers using chlorosilane chemistry, yielding central dendritic cores of spherical shape and different generations on which the desired number of polymeric arms were grafted.[23,24,34] The characteristics of the star-shaped molecules used in this study are shown in Table 1.

Preparation of Star PB Monolayers on Mica. All the samples were prepared by exposing freshly cleaved mica to a toluene solution (good solvent for polybutadiene) of the desired concentration of the star PB. The concentration of the solutions for all the molecules was 100 times less than the critical overlap concentration, i.e., $c/c^* = 0.01$. The c^* was determined from the radius of gyration, R_g, of this star measured in a dilute good solvent solution by light scattering.[26] A variety of incubation times were used, from about 3 min up to 5 days. After incubation the polymer-modified mica was rinsed extensively with toluene and placed in a toluene bath for several hours (>3) to remove any nonadsorbed chains and allow the adsorbed polymers to attain closer to equilibrium conformations. Subsequently, the sample was rapidly dried under flow of nitrogen and imaged in air by AFM in tapping mode.

Atomic Force Microscopy (AFM). All the AFM experiments have been performed in air (bad solvent for the star PB) using a Veeco AFM, multimode/nanoscope IIIa (Veeco, Santa Barbara, CA). The samples were imaged in tapping mode (tip in intermediate contact with the surface). The RTESPA Veeco cantilevers with a nominal spring constant and resonance frequency of 40 N/m and 300 kHz, respectively, were used to image the samples. The cantilevers were oscillated vertically 5% below their natural resonant frequency and moved in a raster fashion within a specified region of interest. Each sample was imaged at several different areas.

Island Volumes, Heights, and Island Surface Coverage Calculations. The free software WSxM (Nanotech Electronica S. L. www.nanotech.es) was used for simple leveling and display. The island heights, volumes, and the surface coverage (percentage of substrate surface covered by polymers) were determined by using either the grain analysis or the roughness analysis module (height distributions of pixels) of the commercial software Scanning Probe Image Processor (SPIP, Image Metrology). The total adsorbed amount, Γ (mg/m^2), was calculated using the observed volumes and the bulk PB density. The volume values calculated directly from AFM image analysis (and consequently the deduced adsorbed amounts) suffer from the convolution effect, which is explained below.

Convolution Effect. AFM images are always a convolution of the geometry of the tip and the shape of the object or sequence of objects being imaged. For the case of an isolated object, the

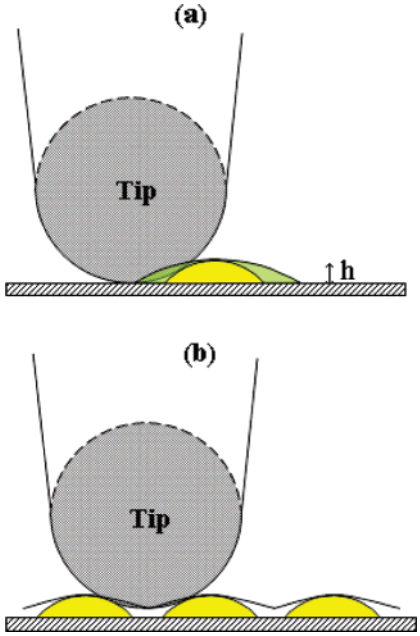

Figure 1. Schematic drawing showing (a) how a spherical cap appears larger due to the convolution of the geometry of the AFM tip and the shape of the object being imaged and (b) how spherical caps sitting next to each other appear shorter, black line.

convolution affects only the lateral dimensions of the object being imaged as the corresponding height is accurately measured (Figure 1a). In general, if the tip is much smaller than the object of observation, the AFM topography will contain minimal artifacts revealing almost the real upper shape of the object. However, common tip apexes are larger than the size of single chains and small groups of chains. Therefore, the convolution effect is significant, and apparent lateral sizes can be larger by an order of magnitude.[7]

For the case of a sequence of objects being close together, i.e., for a high surface density of particles, the convolution due to the geometry of the tip results in images where the height of the objects is underestimated (Figure 1b). This effect has already been reported for the case of a dense monolayer of thiol-terminated polystyrene adsorbed on a gold surface.[12] Deep valleys between the objects are inaccessible to the tip; only the top of the objects can be imaged making the objects appear shorter.

We present a simple calculation in order to approximately estimate the effect of the tip geometry on the measured volume of an object. We assumed that the objects are spherical caps as this has been proven to be a satisfactory assumption for the case of single molecules on surfaces in bad solvent conditions.[7,12] The tip usually has the shape of a pyramid (of a size ~3−5 μm) ending in a sharp apex with an effective radius of curvature (about 40−50 nm for the tips we used in this study as measured by scanning electron microscopy). Using simple geometrical arguments the apparent volume, V_a, of the apparent spherical cap can be connected with the real volume, V_r, of the real spherical cap, the real measured height, h, and the tip radius, R_t.

$$V_a = V_r + \pi h^2 R_t \quad (1)$$

For our calculations we used three different spherical caps of volumes similar to the theoretical volumes of the polymers (in the collapsed state, bad solvent conditions) studied (Table 1). These theoretically estimated volumes (or real volumes), V_r, of the spherical caps were kept constant while the maximum height took values from nearly 0.4 nm (flat conformation) to 16 nm (narrow, vertical conformation), and the convoluted volumes (or apparent volumes), V_a, were calculated. The tip was considered to be a perfect sphere.

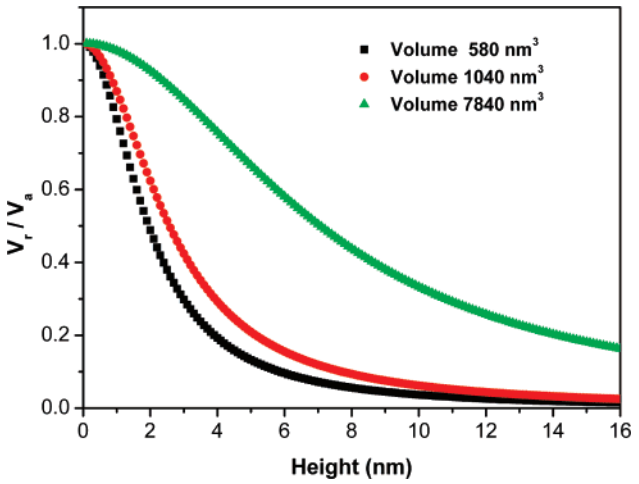

Figure 2. Ratio of the real and the convoluted volume (apparent volume) against the height for three spherical caps of different volumes: (a) 580 nm^3 (black squares), (b) 1040 nm^3 (red circles), and (c) 7840 nm^3 (green triangles) for R_t = 40 nm.

The results from these calculations are presented in Figure 2. They were used to check whether the observed structures/globules represent single collapsed molecules or not. The accurate estimation of the convolution effect for arbitrary shapes of particles and different surface densities is complex. All the volumes and total adsorbed amounts reported here (unless stated otherwise) are *apparent* ones taken directly from AFM images.

Brownian Dynamics Simulations. Snapshots from computer simulations are shown in Figure 15. Full details and analysis will be presented in a future publication.[36] Briefly, coarse-grained models of star polymers adsorbed on a smooth surface were studied using Brownian dynamics simulations. The star polymer structure was described by a bead−spring model, which consists of linear chains of beads connected to a central bead, with each bead bonded to its neighbors with nonlinear springs; more details can be found in the corresponding references.[37−39] The nonbonded bead−bead interaction potential employed was introduced by Steinhauser,[40] which provides a convenient means of tuning the solvent quality from athermal, through ideal-solvent, to bad-solvent conditions. Finally, the smooth surface was described by an effective 9−3 Lennard-Jones potential, which has been used in many applications.[41]

Results

Several samples using different adsorption/incubation times were prepared for each of the different polymers. Several series of 6 × 6 μm^2 images for every sample were collected. Analyzing these images, the average island height, surface coverage and the total adsorbed amount were determined.

In Figure 3, the adsorbed amount against the immersion time for the samples of star polymers with 18 arms, 32 arms, and 59 arms is plotted. It is clear that all the curves follow similar behavior; the adsorbed amount increases monotonically with time and then reaches a plateau. This indicates that there is a specific, to each polymer, maximum adsorbed amount that can be attained at high enough immersion times. In the case of 18 arms the adsorption converged faster to the plateau than for 32 arms, while the adsorption for the 59-arm polymers converged with even slower kinetics.

It should be noted that any quantitative comparison between the maximum adsorbed amount values for the different polymers cannot be easily made due to the difficulty of accounting for the convolution effect. For example, the adsorbed amount of the 18-arm stars is overestimated as the individual islands were well separated and appeared larger (Figure 4). On the other hand, the maximum adsorbed amount for the case of 32 arms and 59

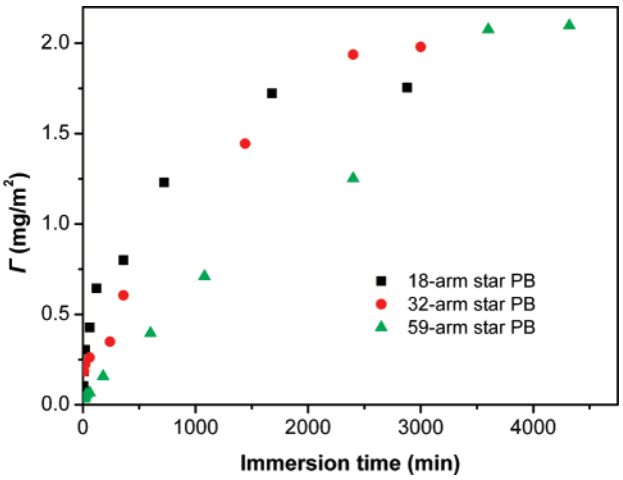

Figure 3. Plot of the adsorbed amount against the immersion time for the samples of star PB with 18 arms (black squares), 32 arms (red circles), and 59 arms (green triangles).

arms could be underestimated since the structures were very close together (Figures 8 and 10); because of the corresponding convolution effect, the islands could appear shorter than they really were, resulting in an artificially lower maximum adsorbed amount. Nevertheless, in spite of these effects, the shape of the adsorption isotherms ensures that the apparent adsorbed amount is a good indicative measure of the increasing adsorption with the immersion time and that we have used sufficiently long immersion times to arrive at an adsorbed amount plateau for all the polymers used.

Figure 4 shows some typical AFM images of 18-arm star PB adsorbed on mica for six selected incubation times, resulting in the adsorbed amounts shown at the top of each image. In Figure 5 we present some high contrast, zoom AFM images. Analyzing at least three images for each immersion time, we measured the corresponding average island height and surface coverage. These values were plotted against the increasing adsorbed amount and are shown in Figure 6. In Figure 4a (see also zoom in Figure 5a) which corresponds to a low incubation time (hence, low adsorbed amount) the polymeric islands appear flat (short), and many of them are noncircular and somewhat elongated on the surface. As the adsorbed amount increased but still for relatively low values (regime I in Figure 6), the height of the islands increased while the surface coverage remained relatively constant. The islands started to appear circular (Figure 4b or zoom in Figure 5b) at the end of regime I. For adsorbed amounts higher than approximately 0.3 mg/m^2 the average height of the islands remained constant while the island coverage increased linearly with the adsorption (regime II in Figure 6). The shape of the islands remained mainly circular, but some asymmetric ones started to appear (Figure 4c). When the adsorbed amount reached a value of about 0.8 mg/m^2, the average height of the islands started again to increase while the surface coverage remained almost constant (regime III in Figure 6). The islands appeared again to take noncircular/elongated shapes and also became wider (Figure 4e,f or Figure 5c).

The volumes of the islands for adsorbed amounts up to around 0.3 mg/m^2 are similar to the convoluted volumes calculated using eq 1. For example, the average island volume measured from the AFM images for an adsorbed amount 0.304 mg/m^2 was about 6500 nm^3 while the calculated convoluted volume using eq 1 (for a real volume equal to the volume of a single collapsed 18-arm star PB, Table 1, and height 4.2 nm) is about 4000 nm^3 (see also Figure 2). Hence, the islands can be considered to be mainly single collapsed star polymers for adsorbed amounts within the regime I in Figure 6. For higher incubation times some bigger islands started to form. For these higher adsorbed amounts we can roughly estimate the number of star molecules in each island by dividing the apparent volume of each island with the apparent volume of the single collapsed star polymer, as it appeared in the low coverage AFM images. In this way, the corresponding probability of finding a set number of molecules in any island can be determined. For example, Figure 7 shows this probability plot for samples with adsorbed amounts at the end of regime I and within regime II.

For an adsorbed amount equal to 0.304 mg/m^2, it is clear that the islands consist mainly of single collapsed stars and in a few cases of few aggregates of two stars. For a higher adsorbed amount (0.429 mg/m^2) the number of single chains decreased while aggregates of three and four stars started to form. For an even higher adsorbed amount (0.644 mg/m^2) the number of single collapsed chains decreased even more while aggregates of three and four stars are more frequent. For yet an even higher adsorbed amount (e.g., 0.801 mg/m^2, not shown), the number of single polymer chains decreased dramatically while the number of multiaggregated chains increased even more, with many of them including 5 or 6 molecules. For high adsorbed amounts, i.e., within the regime III (Figure 6), most polymeric islands can be considered as aggregates of several stars.

Figure 8 shows some typical AFM images of the 32-arm stars adsorbed on mica for six selected incubation times. The average island height and surface coverage were determined by analyzing at least three images for each immersion time we measured. These are plotted vs the adsorbed amount in Figure 9. For a low adsorbed amount the polymeric islands appeared flat on the surface (short) and some of them are asymmetric and elongated (Figure 8a). By increasing the adsorbed amount up to about 0.35 mg/m^2, the average height increased linearly while the island coverage appeared approximately constant (regime I in Figure 9). The shape of the islands started to appear circular at the border between regime I and II. For adsorbed amounts higher than 0.35 mg/m^2 the surface coverage started increasing while the average height of the islands stayed relatively constant, with a small decrease for the highest adsorbed amount measured. The latter could be attributed to the convolution effect due to the formation of a denser structure. For the two highest adsorptions measured (regime III), a semicontinuous network was observed (Figure 8e,f).

For low adsorbed amounts, the volumes of the islands were similar to the convoluted volumes calculated using eq 1. For the adsorbed amount 0.345 mg/μm^2, the measured average volume of the polymeric islands was around 11 000 nm^3 while the theoretical convoluted volume of this molecule is about 7300 nm^3. Hence, the polymeric islands for adsorbed amounts within the regime I in Figure 9 can be considered as mainly single collapsed 32-arm stars. For adsorbed amounts higher than 0.345 mg/μm^2 (regime II of Figure 9), aggregates of 32-arm star molecules started to form, resulting ultimately in the semicontinuous network of Figure 8f (within regime III).

In Figure 10, we present some typical AFM images of 59-arm star PB adsorbed on mica for six selected incubation times. Figure 11 shows the average island height and surface coverage plotted against the adsorbed amount. The island surface coverage increased while the average height of the islands remained nearly constant (about 9 nm), apart from the highest adsorbed amount where the average height decreased (Figure 11). The shape of the islands remained symmetric and circular for all adsorbed amounts. We did not observe any formation of fused aggregates

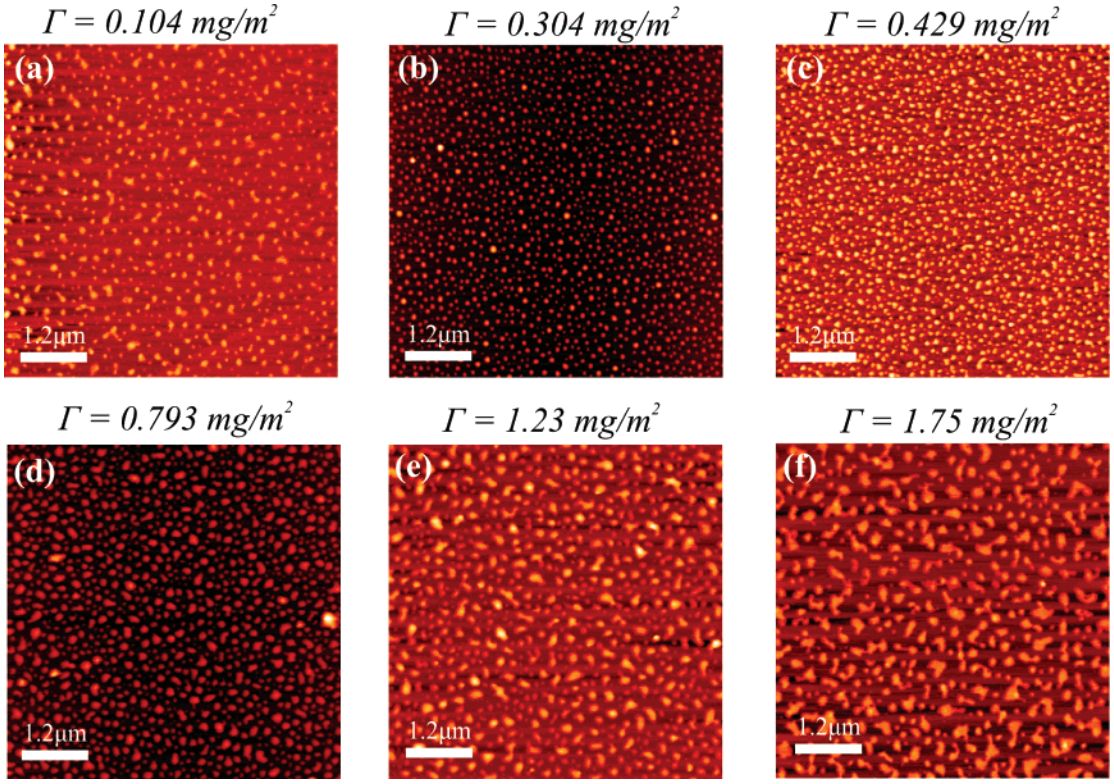

Figure 4. 18-arm star PB molecules adsorbed on freshly cleaved mica from a toluene solution; images in air, 6 × 6 μm^2 scans using tapping mode AFM. The mica was left in the solutions from 3 min up to 2 days. The adsorbed amount of the star PB molecules on mica is given above each image. From images (a) to (f) the adsorbed amount increased from 0.104 up to 1.75 mg/m^2.

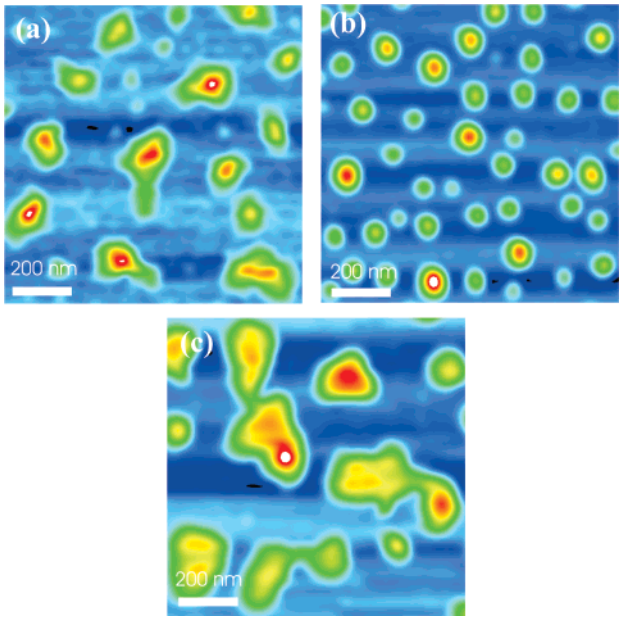

Figure 5. High-contrast AFM images in air, 1 × 1 μm^2. From image (a) to (c) the adsorbed amount is 0.104, 0.304, and 1.75 mg/m^2, respectively.

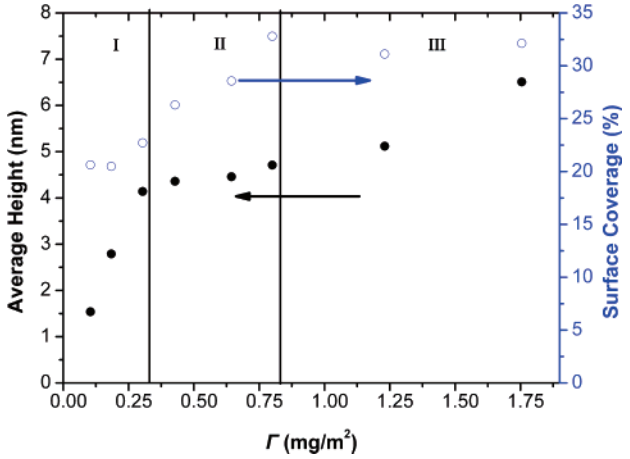

Figure 6. Plot showing the variation of the 18-arm star-PB island average height (black solid points, left scale) and the surface coverage (open blue points, right scale) vs the adsorbed amount. Island average heights and surface coverage data were obtained by averaging the measurements over at least three different areas for each incubation time.

for any adsorbed amounts. The volumes of the islands for most adsorbed amounts (except for the highest one) were similar to the convoluted volumes calculated from eq 1. For example, for the adsorbed amount 0.396 mg/μm^2 the measured/apparent average volume of the polymeric islands was around 34 000 nm^3 while the theoretical convoluted volume of this molecule is about 23 000 nm^3.

Figure 12a shows a high-contrast image of the maximum adsorbed amount (Figure 10f). It is clear that the islands are close together, even touching each other in many cases. The white contours highlight clusters, linear aggregates, and isolated stars. As it has been mentioned in the convolution section, when particles are close together they can appear shorter in an AFM image than they really are. The height distribution of the islands (Figure 12b) has a bimodal character, with the first peak being around 6.5 nm and the second just above 9 nm. This can be explained by the fact that some of the islands were so close together that they appeared shorter, due to the convolution effect, contributing to the first peak of the bimodal distribution while some others did not have any close enough neighbors, and thus their height was not affected, giving rise to the second peak of the bimodal distribution with height of 9 nm. Therefore, the decrease of the average height from around 9 nm to less than

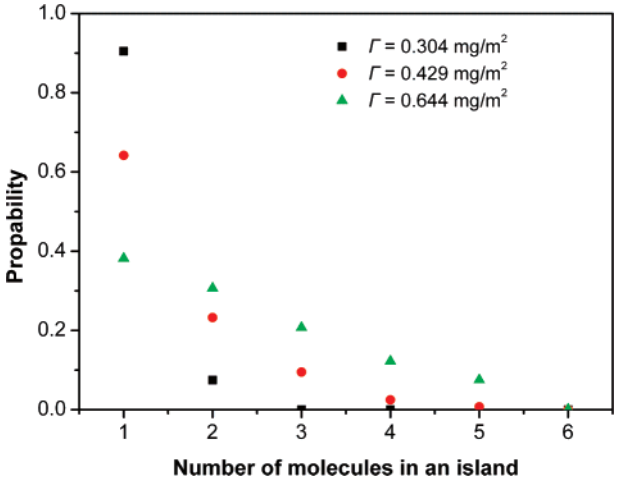

Figure 7. Probability of finding a specific number of polymer chains in an island for $\Gamma = 0.304$ mg/m^2 (black squares), $\Gamma = 0.429$ mg/m^2 (red circles), and $\Gamma = 0.644$ mg/m^2 (green triangles).

8 nm observed for high adsorbed amounts for the case of the 59-arm PB (Figure 11) can be an artifact and a direct consequence of the convolution effect.

In Figure 13, we present the radial averaged intensity (I) of a 2D fast Fourier transform (FFT) of two typical images for each star polymer: one for low and one for the highest observed adsorbed amount. The shape of the FFT is centrosymmetric, implying an isotropic distribution of the islands/structures. The radial averaged intensity shows a maximum at a specified wavevector (q) which corresponds to a characteristic length scale ($\sim 2\pi/q$) for each case, indicating the average distance between nearest neighbors. Similar isotropic distributions hold for almost all of our observed structures when more than ~5 min adsorption times were used (i.e., when a sufficiently large number of molecules were adsorbed). It is worthwhile noting that for the highest adsorbed amount the smallest characteristic length was observed for the intermediate functionality star. Furthermore, moving from a low to the highest adsorbed amount, the characteristic length increased for the 18-arm star polymer while decreased for the 32- and 59-arm star polymers.

Discussion

Adsorption of Star PB on Mica. In Figure 3, the curves of the adsorbed amount against the immersion time of 18-arm, 32-arm, and 59-arm star PB indicate that the higher molecular weight (larger molecular size) polymers exhibited slower adsorption kinetics as one would expect, owing to their slower diffusion coefficient in the solution. The calculation of the exact maximum adsorbed amount from AFM images and hence the exact maximum number of molecules adsorbed on the surface is not easy due to the convolution effect. Nevertheless, in the case of the 59-arm star PB and for high adsorption (Figure 10f), the number of star molecules adsorbed on the surface can be estimated from the corresponding AFM image since each of these globules corresponds to a single collapsed 59-arm star molecule. The number of islands for the highest measured adsorbed amount corresponds to 92 ± 10 particles/μm^2.

Assuming a surface fully covered with hard spheres of radius equal to the star corona radius[22] $R_c = (11/5)^{1/2}R_g = 1.48R_g = 50.5$ nm of the 59-arm star PB (Table 1, good solvent conditions), we can estimate a maximum adsorbed number of particles. For the calculation we assumed the following cases: the densest packing of circles in a plane, the hexagonal lattice,[42] which has a packing density of $n = (1/6)\pi\sqrt{3} = 0.907$; random closed packing[43] (RCP), which gives a packing density of $n = 0.82$; and random loose packing[44] (RLP), $n = 0.772$. For the hexagonal lattice we would expect 113 spheres/μm^2, for RCP, 102 spheres/μm^2, and for RLP, 96 spheres/μm^2. These calculations show that the maximum number of molecules adsorbed on the surface within our experimental protocol compare well with the estimated values for a random packing. This means that at least for the largest f star polymer used in our study the combination of its high osmotic pressure and the repulsive excluded-volume interactions in good solvent conditions does not allow the penetration and adsorption of other molecules within the pervaded volume of the already adsorbed ones; i.e., the overlap surface density in good solvent conditions is the maximum density that can be attained on the surface using our experimental protocol.

Growth of Star PB Monolayers on Mica. We will divide the discussion for the monolayer growth on mica in three parts: regime I: low adsorbed amount region; regime II: intermediate adsorbed amount region; and regime III: high adsorbed amount region. In Figure 14 we plot separately the average island height and surface coverage for all polymers, noting the extent and boundaries of each regime.

(i) Regime I: Low Adsorbed Amounts. At first, we concentrate on the lowest adsorbed amount observed in our experiments for each case; $\Gamma = 0.104$ mg/m^2, $\Gamma = 0.185$ mg/m^2, and $\Gamma = 0.058$ mg/m^2 for 18-, 32-, 59-arm star PB, respectively.

In general, the structure of polymers adsorbed on surfaces in good solvent conditions depends strongly on the surface polymer density due to the repulsive excluded-volume interactions with the surrounding adsorbed chains.[45] In the case of 18-arm and 32-arm star polymers and for the lowest adsorption presented here the numbers of the adsorbed chains are similar, 16 ± 3 and 14 ± 2 chains/μm^2, respectively. If we assume that the molecules were homogenously and isotropically distributed on the surface when in good solvent conditions (before the abrupt solvent evaporation), the average distance between the centers of the molecules would be between 250 and 300 nm, which is of the order of their sizes if their arms are fully stretched. The same applies for the 59-arm star PB for the case of the lowest adsorbed amount. Hence, we can assume that the interactions among them are weak.

Asphericity in the shape of single star polymers in bulk good solvent conditions has been reported in molecular dynamics (MD) simulations: an evolution of the star polymer conformation from an aspherical to spherical object with increasing functionality was observed.[21,22] In our experiments we have observed the same trend albeit for surface conformations in the dry state. We suggest that the degree of asymmetry observed in these conditions could be due to the different degree of asphericity/asymmetry when the adsorbed polymers were in good solvent conditions. For the lower functionality star polymers, their asymmetry in good-solvent conditions was captured in the dry state when the molecule abruptly collapsed due to the rapid evaporation of the solvent. In contrast, the 59-arm star polymer is expected to be relatively spherical in good solvent conditions due to its high functionality, leading to a symmetric, circular collapsed conformation. This interpretation indicates that the shape and size (parallel and normal to the surface) of the collapsed star polymer depend strongly on the conformation of the adsorbed star polymer in the initial good solvent conditions just before drying.

At the lowest adsorbed amount, the height of the 18-arm star globules was ~1.5 nm (Figure 6 or 14). It has to be noted that a similar height has been observed for isolated collapsed linear

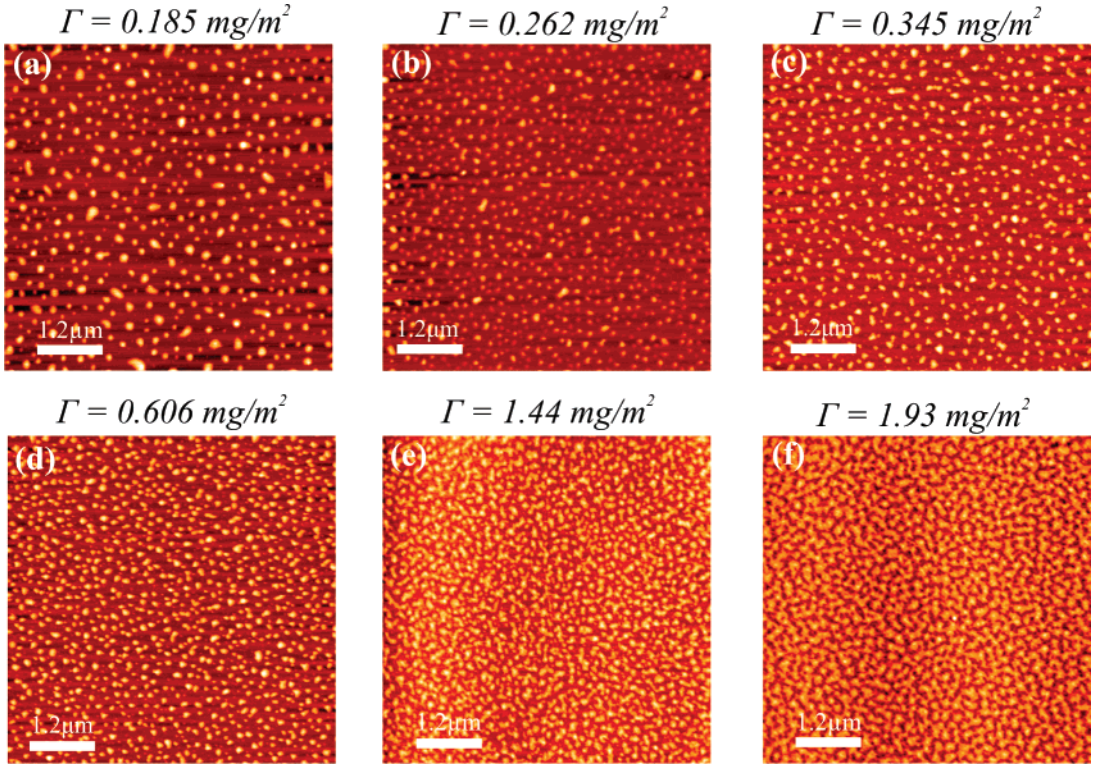

Figure 8. 32-arm star PB molecules adsorbed on freshly cleaved mica from a toluene solution; images in air, 6 × 6 μm^2 scans using tapping mode AFM. The mica was left in the solutions from 5 min up to ~2 days. The adsorbed amount of the star PB polymers on mica is given above each image. From image (a) to (f) the adsorbed amount increased from around 0.185 up to 1.93 mg/m^2.

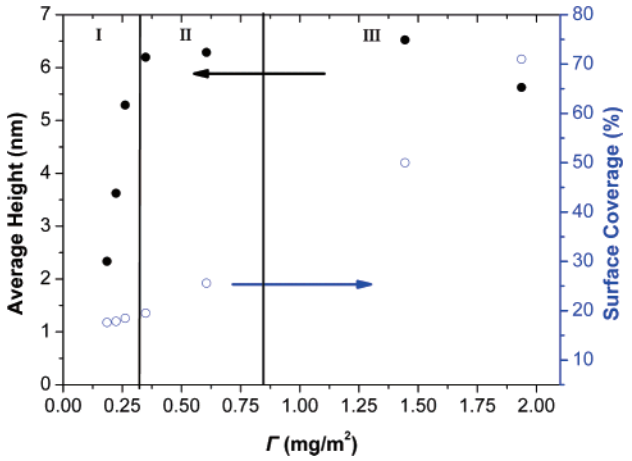

Figure 9. Plot showing the variation of the 32-arm star-PB island average height (black solid points, left scale) and the surface coverage (open blue points, right scale) vs the adsorbed amount. Island average heights and coverage data were obtained by averaging the measurements over at least three different areas for each incubation time.

PB chains of different molecular weights in air.[46] For the 32-arm star the average height of the single molecules appeared to be higher, ~2.3 nm (Figure 9 or 14), while for the 59-arm star the measured height appeared much higher, ~9 nm (Figure 11 or 14). These observations clearly show that the height of isolated adsorbed collapsed star polymers depends strongly on their functionality. In general, a single physisorbed linear homopolymer gains energy of δkT with each surface contact. Although δ in most cases is much smaller than unity, it is energetically favorable for the molecule to form many contacts with the surface and attain a total energy much larger in magnitude than kT (larger than its entropic contribution to free energy), resulting in a flat conformation.[47] Similarly, an isolated star physisorbed polymer would try to balance the loss of entropy due to confinement with the decrease in energy by both (i) adsorbing many arms and (ii) increasing the number of monomer contacts of each adsorbed arm with the surface. However, each arm conformation is affected by the excluded-volume interactions with the other arms of the same star which are joined together in its center. This intramolecular crowding effect is expected to play a particularly important role for star polymers with a high functionality and explains their increased height. We can quantify this effect by defining the fraction of nonadsorbed monomers of the star polymer, Φ_{na} (i.e., Φ_{na} is the ratio of the monomers not in contact with the surface over the total number of monomers of the star polymer). Owing to the crowding effect, in good solvent conditions the increase of the star polymer functionality results in an increased number of nonadsorbed chain arms and consequently in an increase of Φ_{na}. Additionally, the nonadsorbed arms would be more stretched for higher functionality stars due to the increased local density and the repulsive monomer−monomer excluded-volume interactions, in analogy with the well-known polymer "brush" where the increase of the surface grafting density results in a thicker swollen brush with the chains stretched away from the surface (balanced only by their entropic elasticity).[48] Therefore, the height of the adsorbed star polymer should be larger for higher functionalities in good solvent conditions. Preliminary results of a Brownian dynamic simulation study (Figure 15) have indeed shown that higher functionality stars adsorbed on a surface exhibit higher Φ_{na} in good solvent conditions. When the solvent conditions change from good to bad, the chain arms collapse trying to minimize their contact with the air. Each arm will collapse in a way that depends on whether it is adsorbed or not. If the arm is adsorbed it will try to keep many contact points with the surface to retain the favorable adsorption energy. The nonadsorbed arms will collapse together, forming a polymer globule/nanodroplet (trying to minimize the contact with the air) on top of the adsorbed chain-arm "layer". Consequently,

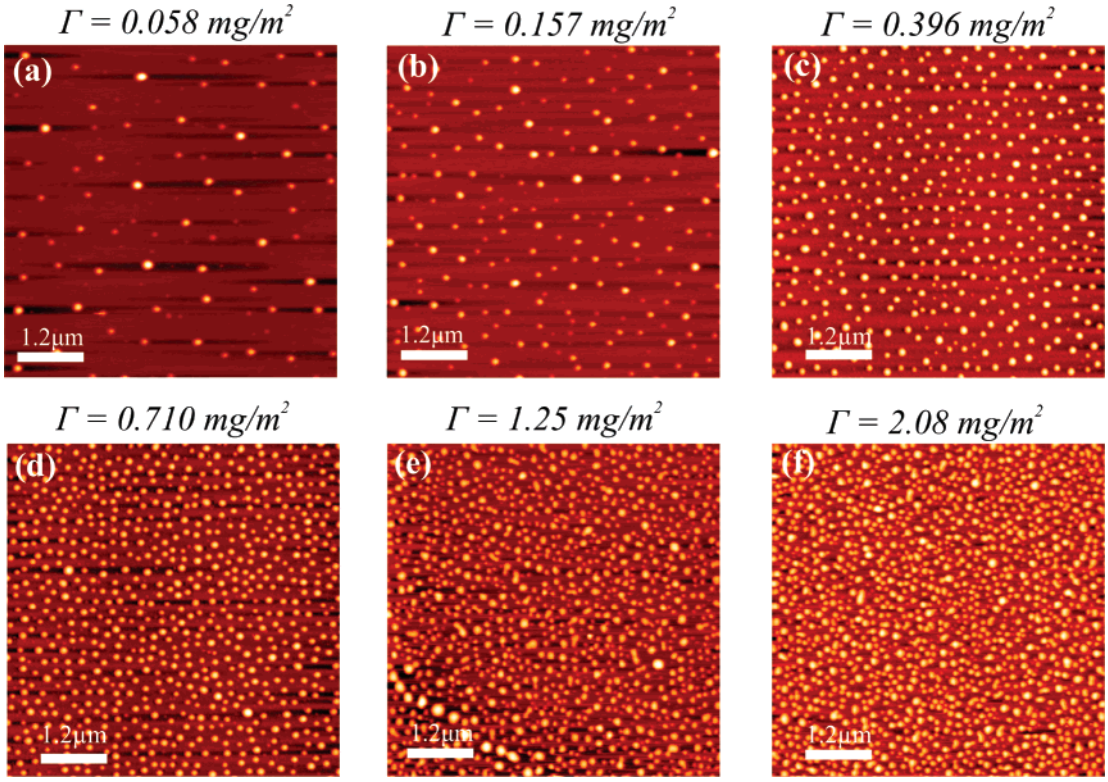

Figure 10. 59-arm star-PB molecules adsorbed on freshly cleaved mica from a toluene solution; images in air, 6 × 6 μm^2 scans using tapping mode AFM. The mica was left in the solutions from 5 min up to 3 days. The adsorbed amount of the star PB molecules on mica is given above each image. From image (a) to (f) the adsorbed amount increased form 0.058 up to 2.08 mg/m^2.

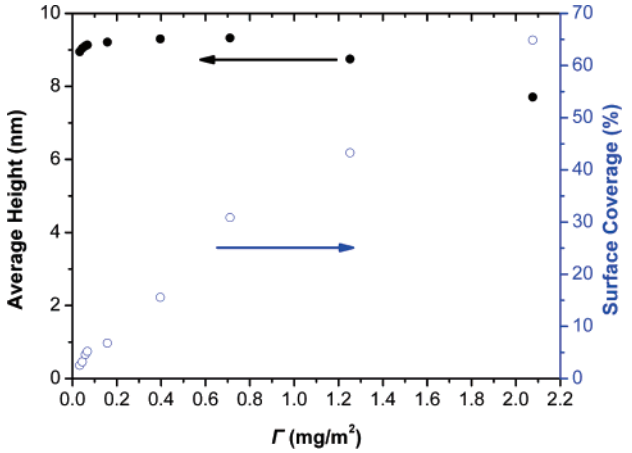

Figure 11. Plot showing the variation of the 59-star PB island average height (black solid points, left scale) and the surface coverage (open blue points, right scale) vs the adsorbed amount. Island average heights and coverage data were obtained by averaging the measurements over at least three different areas for each immersion time.

the height of the globule is expected to be larger for higher Φ_{na} and hence for stars with higher functionality. This leads to higher collapsed globules for stars with higher functionalities when the solvent conditions change (Figure 15, right).

By increasing the adsorbed amount, the average height of the single star globules increased for the 18-arm and 32-arm star PB, while for the 59-arm the average height increased only slightly. In regime I, the increase of the adsorbed amount resulted in the decrease of the average distance between the adsorbed molecules, leading to higher local densities and due to the repulsive excluded-volume interactions between the molecules in good solvent conditions to a confinement effect. The available space for each adsorbed star polymer decreased, leading to a reconformation of the adsorbed chains to higher loop and tail distributions and possibly to (at least partial) desorption of some chain arms; these changes led to an increase of Φ_{na}. Higher Φ_{na} results in higher and narrower collapsed globules. This effect explains the height increase of the 18-arm star and 32-arm PB in this regime. Moreover, this confinement and reconformation effect also explains why the collapsed globules appeared more symmetric/circular (Figure 4b or 5b and Figure 8c) than in the case of the lowest adsorbed amount. The island surface coverage remained relatively constant while the adsorbed amount increased, since the increase of the number of molecules adsorbed on the surface was balanced from the fact that the corresponding collapsed molecules were narrower and occupied less space laterally.

The proposed reconformation for the 59-arm star polymer is expected to be less important since the star stiffness increases with functionality: the intramolecular structure would not be significantly affected from the intermolecular (star−star) excluded-volume repulsions in good solvent conditions, and hence the molecule would collapse into a globule with dimensions (both in height and laterally) largely independent of the adsorbed amount. In agreement with these arguments, our results indeed show that the height of the individual 59-arm star globules increased only slightly with the adsorbed amount while the island surface coverage increased as more stars were adsorbed (Figures 11 and 14).

If we compare the space available for each individual molecule within the region of low adsorbed amounts, we find that the values are significantly larger than the size of the molecule in (bulk) good solvent conditions $2R_c = 2\,(11/5)^{1/2}R_g = 2.96R_g$. In all star polymer cases for the highest adsorbed amount within this regime, the ratio of the bulk R_c to the effective average half distance between the molecules (calculated from AFM images) takes values close to 0.3. This is not so surprising since an adsorbed molecule is expected to take

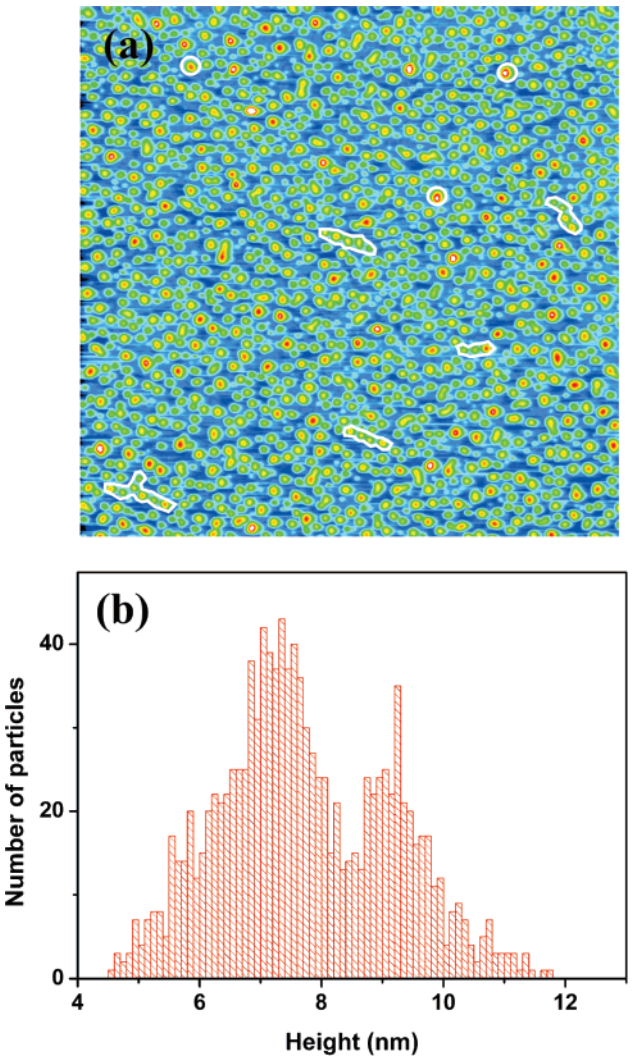

Figure 12. (a) High-contrast image (6 × 6 μm^2) and (b) height distribution of the islands for the sample of 59-arm PB with $\Gamma = 2.08$ mg/m^2.

laterally an extended conformation owing to (i) the energetically favorable contacts with the surface leading to a relatively extended flat shape and (ii) the increased intramolecular crowding effect (compared to a bulk solution) combined with the repulsive excluded-volume interactions since many chain arms have to be accommodated within a 2D space.

(ii) Regime II: Intermediate Adsorbed Amounts. Increasing further the adsorbed amount for 18- and 32-arm star PB, the average island height remained constant. This constant value for the 18-arm star PB was ∼4.5 nm while for the 32-arm star PB was ∼6.3 nm (Figure 14).

The average island height of about 4.5 nm for the case of the 18-arm star PB was reached at about $\Gamma = 0.3$ mg/m^2 (Figure 4b or 5b, end of regime I). From island volume analysis, we deduced that these islands correspond mainly to single collapsed molecules. By increasing the adsorbed amount, some aggregates of star polymers started to form. Because of the low functionality, the osmotic pressure of these star polymers is low, and increasing the number of stars resulted in interpenetration between them and thus in the formation of aggregates upon the sudden evaporation of the solvent; i.e., they collapsed together when the monomer−monomer interactions changed from repulsive (good solvent conditions) to attractive (bad solvent conditions). Increasing the adsorbed amount, more aggregates with higher number of molecules within the aggregates formed (Figure 7). The average island height did not change significantly, indicating that their interpenetration in this regime was relatively small. This behavior led to the increase of the surface coverage with the increase of the adsorbed amount in regime II.

For 32-arm star PB similar effects were observed, and similar interpretation arguments can be made. However, in this case the interpenetration between different stars is expected to be less as the osmotic pressure within the 32-arm star is higher than in the case of the 18-arm one. Few aggregates started to form for $\Gamma = 0.606$ mg/m^2 (Figure 8d), and their number and size increased for higher adsorbed amounts. The average height of the collapsed polymeric islands remained approximately constant (Figure 9 or 14). In turn, this led to an increase of the island coverage of the surface with the increase of the adsorbed amount.

For the star PB with 59 arms, the average height of the islands did not change (Figure 11 or 14), and no aggregation was observed. The 59-arm star polymers can be considered relatively hard and are not affected from the confinement/crowding effect due to the increase of the adsorbed amount. Moreover, owing to the relatively high osmotic pressure inside the star, interpenetrations are more difficult to occur and no aggregates were observed. Hence, the surface coverage increased linearly with the adsorbed amount.

(iii) Regime III: High Adsorbed Amounts. For the 18-arm star the islands within this regime correspond mainly to aggregates of several chains. The number of the associated star molecules within the aggregates increased with the adsorbed amount. Owing to the closer packing in good solvent conditions, the interpenetrations between the star polymers were larger, leading to partial fusion upon the change of the solvent conditions. Hence, the height of the collapsed aggregates became larger (Figure 6 or 14) as progressively higher interpenetrations occurred. Although the adsorbed amount increased and hence more particles had adsorbed on the surface, the surface coverage remained relatively constant (Figure 6 or 14). AFM images (d), (e), and (f) in Figure 4 show the presence of fewer islands but they are laterally larger, balancing the total surface coverage. At the highest adsorbed amount, the structure adopts the form of a discontinuous pattern of asymmetric islands of aggregates (Figure 4f or 5c). Although low functionality stars allow large interpenetrations, still the specificity of the star architecture does not allow a full penetration. Thus, they retain to some extent their individuality, preventing the formation of symmetric/circular aggregates (observed in the case of linear chains[46]) under bad solvent conditions.

In the case of the 32-arm star PB, aggregates started to form (Figure 8e) with average height similar to the island height at intermediate adsorbed amounts (Figure 9 or 14). At the very highest adsorbed amount the height is slightly smaller but as discussed there is an underestimation due to convolution effects. At this adsorbed amount the island growth led to a dense semicontinuous network of elongated narrow stripes (Figure 8f). Their width is comparable to the width of single collapsed 32-arm PB chains, and the total surface coverage is much higher (almost double) than in the case of the 18-arm polymer. The higher functionality stars have higher osmotic pressure and thus lower ability for interpenetrations and consequently more colloid-like behavior. Thus, they take laterally less extended conformations, and they connect laterally only to few neighbors, forming these linear semicontinuous aggregation patterns in analogy to two-dimensional stripe-like structures predicted in simulations.[49,50] It has to be noted that these simulations predict stripe-like structures stemming from purely repulsive interactions

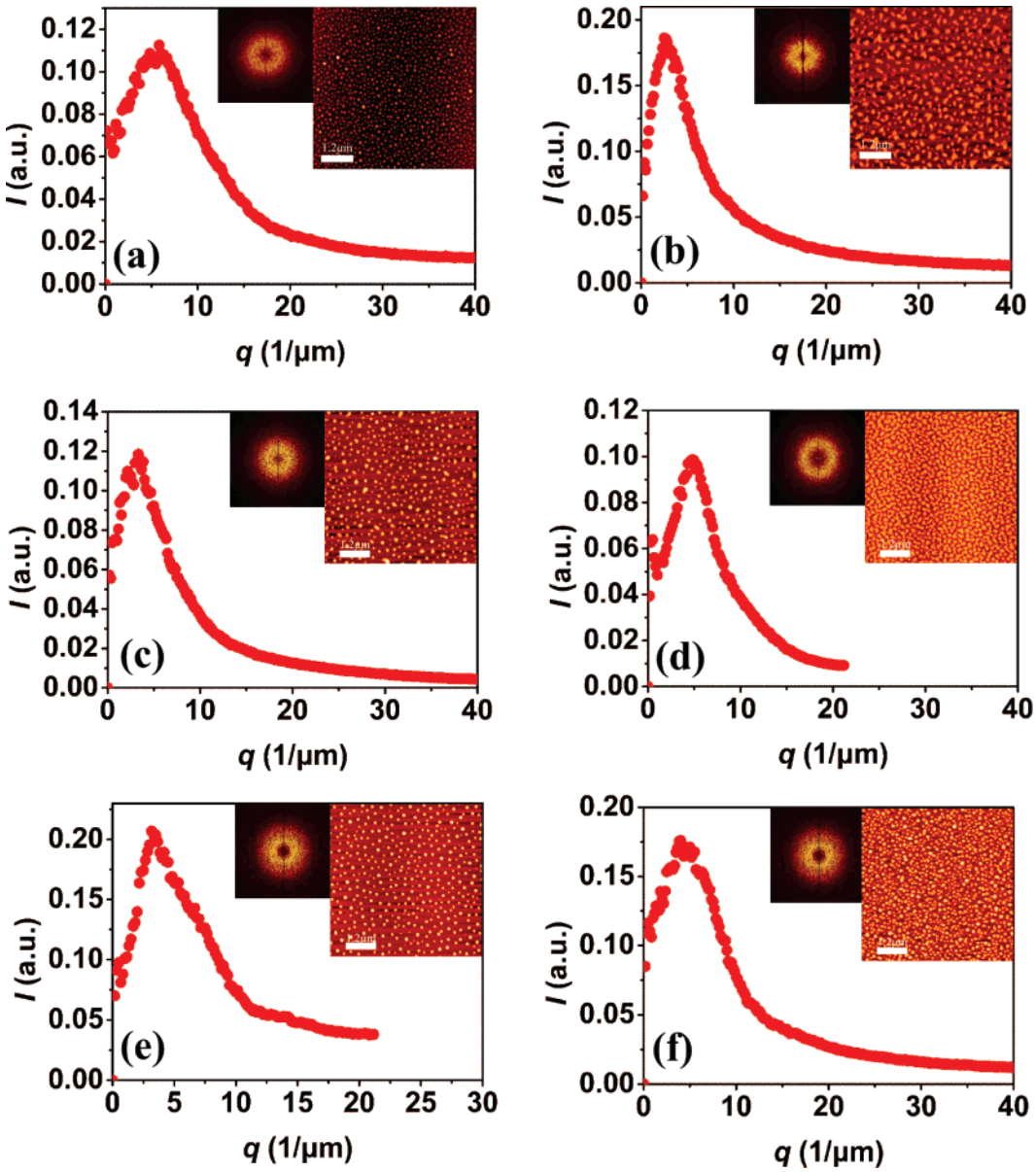

Figure 13. Relative average intensity (I) as a function of the wave number ($q = 2\pi/\lambda$) for star PB of (a) 18 arms and $\Gamma = 0.304$ mg/m^2, (b) 18 arms and $\Gamma = 1.75$ mg/m^2, (c) 32 arms and $\Gamma = 0.185$ mg/m^2, (d) 32 arms and $\Gamma = 1.94$ mg/m^2, (e) 59 arms and $\Gamma = 0.396$ mg/m^2, and (e) 59 arms and $\Gamma = 2.08$ mg/m^2. These plots were obtained by the radial average of the 2D FFT image (small inset, left) resulting from the corresponding AFM image (large inset, right) and show a maximum at a specific wave vector q which corresponds to a characteristic length scale of 171, 389, 300, 204, 311, and 255 nm for images (a) to (f), respectively.

between particles "consisting of an exclusion zone plus a fine shoulder",[49] which can be a simplified model of the repulsion associated with soft particles such as star polymers with sufficient number of arms. This raises the possibility that these structures were formed on the surface under good solvent conditions before the evaporation of the solvent. However, there is also the possibility that these patterns arise upon the evaporation of the solvent due to the resulting attractive interactions in the dry state. Measurements in good solvent conditions are required to clarify this issue which is beyond our current study, and they will be pursued in the future. It should be noted that irrespective of the underlying mechanism for the formation of this structure, its percolating character is of particular interest. Our measurements indicate that at some surface density and a critical f value (and consequently at a critical effective particle stiffness) a percolating structure occurs.

The colloid-like behavior is even more pronounced in the case of the 59-arm star PB where even for the highest observed adsorbed amount the stars keep their individualty, and the aggregation takes a soft colloid-like character. In this case, the very high functionality leads to a very high osmotic pressure within the star, reducing further the interpenetrations of the star arms in good solvent conditions. This effect prevents extended fusion within the aggregates under bad solvent conditions. Although a number of small stripes can also be seen for the 59-arm star (Figure 12), the overall structure is quite different than the one observed for the 32-arm star since both colloid-like clusters and some single stars were observed. This structure was obtained from a surface concentration close to overlap in good solvent conditions. Thus, for such high functionalities, it is reasonable to assume that a glassy state (in good solvent conditions) has been reached due to a kinetic arrest of the stars. This might be the origin of the absence of the percolating structure observed for 32 arms. Our experiments suggest that the critical arm number for such a transition on adsorbed star polymers is between 32 and 59. This is a smaller than the

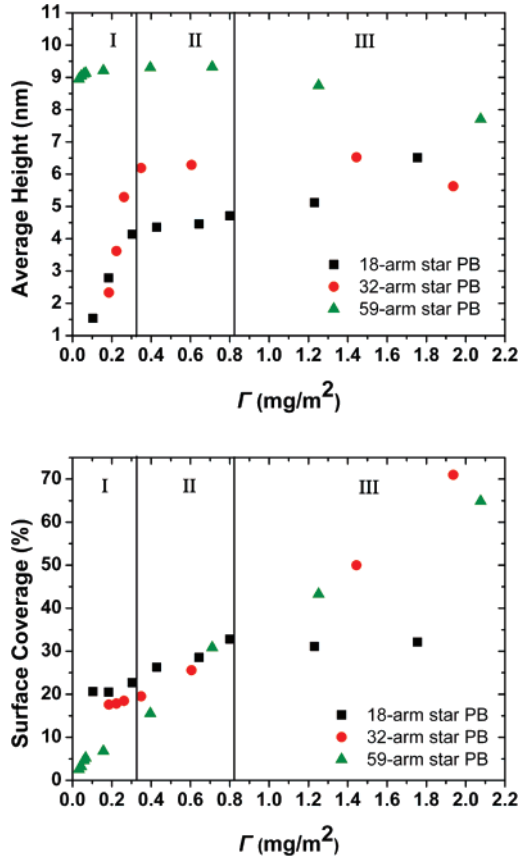

Figure 14. (top) Island average height vs adsorbed amount and (bottom) surface coverage vs adsorbed amount for 18-arm (black squares), 32-arm (red circles), and 59-arm (green triangles) star PB. Regimes I, II, and II are depicted in each plot.

corresponding value for the onset of a glassy state in 3D bulk solution,[29,30] which is a clear manifestation of the strong confinement effect of the surface.[31] The average height again slightly decreased compared to the heights associated with the intermediate adsorbed amounts, but this is also explained in terms of the AFM convolution effect.

It is interesting to note that for the highest grafting densities the smallest characteristic length (Figure 13) was observed for the 32-arm star. This is due to the fact that its functionality is not low enough to promote easy interpenetration and consequently large isolated aggregates (as in the case of 18-arm star) and not high enough to reduce interpenetrations to such a degree that allows stars to behave as soft colloidal particles (as in the case of 59-arm star). The preference for large isolated aggregates in the case of the low functionality polymer results in a relatively large characteristic length (at the highest adsorbed amount) compared to the characteristic length at low adsorbed amount.

Isotropic Order. As we have seen in Figure 13, the polymers have acquired isotropic distributions on the surface, revealing some "liquid-like" ordering behavior. It is highly unlikely that this effect is related to solvent instabilities due to its rapid evaporation (last step before imaging in dry conditions); rapid evaporation of the solvent in various polymers on surface systems has not been shown to affect the positions of adsorbed molecules.[9,10,14] If the resulting structures are purely due to the dewetting of the solvent and the stars play only a passive role (i.e., being dragged by a dewetting liquid instability), then the structures should have been quite similar and relatively independent of adsorbed amount (above a certain limit) and independent of star molecular weight and functionality (since the drying rate is the same for all samples). Thiele et al. in their study on dewetting patterns of evaporating thin liquid films[51] reported that the molecular weight of molecules did not influence their observed surface structures, proving that in dewetting the patterns are an intrinsic property of the solvent. It is worth to mention that in their study they observed heterogeneous nucleated holes (diameter $\sim$ 400 nm) even for thin films and fast solvent evaporation rate. In our AFM images no holes were observed (for any adsorbed amount and any star functionality). However, at the last stages of the drying process it is reasonable to assume that due to the affinity between the polymer and the solvent, some solvent molecules were trapped within and around the polymers. The associated capillary forces could play a role in the aggregation behavior, especially when the polymer surface density is relatively high. Furthermore, the trapped solvent could increase the polymer mobility (plasticizing effect) and could facilitate the nanostructure formation. Nevertheless, even if the clustering was somewhat affected by the capillary forces, the different chain−chain interactions originating from the different functionalities played the major role since we see a clear dependence of interpenetration and clustering behavior on functionality alone.

Consequently, it is more likely that the observed isotropic order in bad-solvent conditions stems from an isotropic arrangement of the star chains in good-solvent conditions. In our system during adsorption and even more importantly during the immersion of the sample in a pure toluene bath for several hours, the polymers have acquired equilibrated arrangements (positions and conformations). In other words, our results suggest that the adsorbed polymers are capable of reconfiguring their position and conformation when in good solvent for sufficiently long times, exploring the available space on the surface and "feeling" to some extent their neighbors at sufficiently high surface coverage. This might be due to the fact that although at the whole chain scale the molecule is expected to be relatively strongly adsorbed through the many monomer contacts with the surface, at the monomer scale the adsorption is relatively weak (to be expected for the nonspecific interactions between mica and PB), and dynamic monomer adsorption−desorption effects can easily occur when in good solvent, leading to a slow but finite mobility of the whole molecule on the surface. In support of our arguments, we note that the ordered structures we obtained are reminiscent of some ordered heteroarm star polymer morphologies originating from Langmuir−Blodgett monolayers (within which the mobility at the liquid−air interface is certainly enhanced)[17] while they are very different to the relatively disordered (at the long and medium range) structures of polymers which have not been subjected to a good solvent bath treatment.[9] This means that our adsorbed polymers when in good solvent behaved like a two-dimensional system of repulsive soft spheres; indeed, some of our structures (e.g., Figure 8f) are similar to theoretical predictions of "stripe phases from isotropic repulsive interactions".[49,50] It is also worthwhile noting that our results show that the formation of dimple (Figures 8d and 10f) and/or ripple (Figure 8e,f) morphologies is not an exclusive property of mixed block copolymer (linear[10] or star[16]) brushes but can also be observed in homopolymer systems such as ours at sufficiently high surface densities. It has to be noted that our experimental protocol does not allow the development of surface densities much higher than the overlap density ($\sigma \gg \sigma^*$) in which for high functionalities more regular structures are expected to form.

Conclusions

Structures of star polymers adsorbed on flat surfaces from a good solvent were studied by atomic force microscopy in the

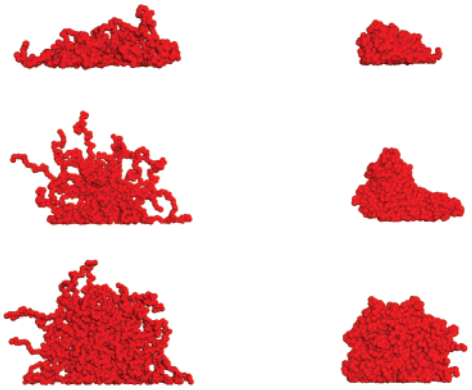

Figure 15. Snapshots of a Brownian dynamic (BD) simulation displaying the different conformations of a star polymer with different functionality adsorbed on a surface in good-solvent conditions (left) and the corresponding conformation of the collapsed star polymer in bad-solvent conditions (right). From top to bottom the star functionality increases, $f = 18$, 32, and 64, leading to a higher number of swollen nonadsorbed arms in good-solvent conditions (left) and to higher collapsed globules in bad-solvent conditions (right). A systematic study is under preparation.

dry state. (i) At sufficiently low surface densities, we observed isolated stars, which for low functionalities (18, 32) acquired flat conformations whereas for the higher one (59) the overall shape is reminiscent of a soft colloid. We have argued that this behavior stems from an intramolecular crowding effect related to the multiple arms. Increasing the surface density, the results indicate a molecular reorganization for low functionality stars due to an intermolecular crowding effect and their low internal osmotic pressure. The higher functionality (59) star appeared unperturbed. (ii) The increased interactions at intermediate surface densities for the low functionality star (18) resulted in interpenetrations leading to aggregation while for higher functionalities (32, 59) interpenetration was not significant. (iii) At even higher surface densities, increased and/or multiple interpenetrations for the low functionality stars led to the formation of elongated discontinuous islands (18 arms) or semicontinuous networks of connected molecules (32 arms). The high functionality star polymer (59) continued to behave as a soft colloid, keeping its individuality within its aggregates. We have argued that its surface structure in the dry state originated from an arrested glassy state at close to overlap concentration in good solvent. For all functionalities, at sufficiently high surface densities, an isotropic distribution of adsorbed polymer was observed, indicating near to equilibrium positions and conformations just before the sudden change of solvent conditions.

Acknowledgment. The authors are grateful to Jacques Roovers for the synthesis of the star polymers and for helpful suggestions. E.G. acknowledges financial support from EPSRC DTA and the Institute for Materials and Processes, School of Engineering and Electronics at the University of Edinburgh. A.C. thanks the School of Chemistry at the University of Edinburgh for financial support.

References and Notes

(1) Napper, D. H. *Polymeric Stabilization of Colloidal Dispersions;* Academic Press: London, 1983.
(2) Gast, A. P.; Leibler, L. *Macromolecules* **1986**, *19*, 686−691.
(3) Cox, J. K.; Eisenberg, A.; Lennox, R. B. *Curr. Opin. Colloid Interface Sci.* **1999**, *4*, 52−59.
(4) Pludeman, E.; Collins, N. *Adhesion Science and Technology;* Plenum Press: New York, 1975; Vol. 9a.
(5) Migler, K. B.; Hervet, H.; Leger, L. *Phys. Rev. Lett.* **1993**, *70*, 287−290.
(6) Brown, H. R. *Science* **1994**, *263*, 1411−1413.
(7) Koutsos, V.; van der Vegte, E. W.; Grim, P. C. M.; Hadziioannou, G. *Macromolecules* **1998**, *31*, 116−123.
(8) Zhao, J. C.; Tian, S. Z.; Wang, Q.; Liu, X. B.; Jiang, S. C.; Ji, X. L.; An, L.; Jiang, B. Z. *Eur. Phys. J. E* **2005**, *16*, 49−56.
(9) Kiriy, A.; Gorodyska, G.; Minko, S.; Jaeger, W.; Stepanek, P.; Stamm, M. *J. Am. Chem. Soc.* **2002**, *124*, 13454−13462.
(10) Minko, S.; Kiriy, A.; Gorodyska, G.; Stamm, M. *J. Am. Chem. Soc.* **2002**, *124*, 3218−3219.
(11) Koutsos, V.; van der Vegte, E. W.; Hadziioannou, G. *Macromolecules* **1999**, *32*, 1233−1236.
(12) Koutsos, V.; van der Vegte, E. W.; Pelletier, E.; Stamouli, A.; Hadziioannou, G. *Macromolecules* **1997**, *30*, 4719−4726.
(13) Li, X.; Han, Y. C.; An, L. J. *Langmuir* **2002**, *18*, 5293−5298.
(14) Gorodyska, G.; Kiriy, A.; Minko, S.; Tsitsilianis, C.; Stamm, M. *Nano Lett.* **2003**, *3*, 365−368.
(15) Kiriy, A.; Gorodyska, G.; Minko, S.; Tsitsilianis, C.; Jaeger, W.; Stamm, M. *J. Am. Chem. Soc.* **2003**, *125*, 11202−11203.
(16) Lupitskyy, R.; Roiter, Y.; Tsitsilianis, C.; Minko, S. *Langmuir* **2005**, *21*, 8591−8593.
(17) Gunawidjaja, R.; Peleshanko, S.; Genson, K. L.; Tsitsilianis, C.; Tsukruk, V. V. *Langmuir* **2006**, *22*, 6168−6176.
(18) Kiriy, A.; Gorodyska, G.; Minko, S.; Stamm, M.; Tsitsilianis, C. *Macromolecules* **2003**, *36*, 8704−8711.
(19) Peleshanko, S.; Jeong, J.; Gunawidjaja, R.; Tsukruk, V. V. *Macromolecules* **2004**, *37*, 6511−6522.
(20) Seghrouchni, R.; Petekidis, G.; Vlassopoulos, D.; Fytas, G.; Semenov, A. N.; Roovers, J.; Fleischer, G. *Europhys. Lett.* **1998**, *42*, 271−276.
(21) Grest, G. S.; Fetters, L. J.; Huang, J. S.; Richter, D. *Adv. Chem. Phys.* **1996**, *94*, 67−163.
(22) Likos, C. N. *Phys. Rep.* **2001**, *348*, 267−439.
(23) Zhou, L. L.; Hadjichristidis, N.; Toporowski, P. M.; Roovers, J. *Rubber Chem. Technol.* **1992**, *65*, 303−314.
(24) Roovers, J.; Zhou, L. L.; Toporowski, P. M.; Vanderzwan, M.; Iatrou, H.; Hadjichristidis, N. *Macromolecules* **1993**, *26*, 4324−4331.
(25) Daoud, M.; Cotton, J. P. *J. Phys. (Paris)* **1982**, *43*, 531−538.
(26) Vlassopoulos, D.; Fytas, G.; Pakula, T.; Roovers, J. *J. Phys.: Condens. Matter* **2001**, *13*, R855−R876.
(27) Likos, C. N.; Lowen, H.; Watzlawek, M.; Abbas, B.; Jucknischke, O.; Allgaier, J.; Richter, D. *Phys. Rev. Lett.* **1998**, *80*, 4450−4453.
(28) Watzlawek, M.; Likos, C. N.; Lowen, H. *Phys. Rev. Lett.* **1999**, *82*, 5289−5292.
(29) Stiakakis, E.; Vlassopoulos, D.; Loppinet, B.; Roovers, J.; Meier, G. *Phys. Rev. E* **2002**, *66*, 051804.
(30) Vlassopoulos, D. *J. Polym. Sci., Part B: Polym. Phys.* **2004**, *42*, 2931−2941.
(31) Jusufi, A.; Dzubiella, J.; Likos, C. N.; Von Ferber, C.; Lowen, H. *J. Phys.: Condens. Matter* **2001**, *13*, 6177−6194.
(32) Joanny, J. F.; Johner, A. *J. Phys., II* **1996**, *6*, 511−527.
(33) Striolo, A.; Prausnitz, J. M. *J. Chem. Phys.* **2001**, *114*, 8565−8572.
(34) Toporowski, P. M.; Roovers, J. *J. Polym. Sci., Part A: Polym. Chem.* **1986**, *24*, 3009−3019.
(35) Roovers, J. *Macromolecules* **1994**, *27*, 5359−5364.
(36) Chremos, A.; Glynos, E.; Koutsos, V.; Camp, P. J., manuscript in preparation.
(37) Grest, G. S.; Kremer, K. *Phys. Rev. A* **1986**, *33*, 3628−3631.
(38) Grest, G. S.; Kremer, K.; Witten, T. A. *Macromolecules* **1987**, *20*, 1376−1383.
(39) Jusufi, A.; Watzlawek, M.; Lowen, H. *Macromolecules* **1999**, *32*, 4470−4473.
(40) Steinhauser, M. O. *J. Chem. Phys.* **2005**, *122*, 094901.
(41) Sides, S. W.; Grest, G. S.; Stevens, M. J. *Macromolecules* **2002**, *35*, 566−573.
(42) Steinhaus, H. *Mathematical Snapshots*, 3rd ed.; Dover Publications: New York, 1999.
(43) Bideau, D.; Gervois, A.; Oger, L.; Troadec, J. P. *J. Phys. (Paris)* **1986**, *47*, 1697−1707.
(44) Hinrichsen, E. L.; Feder, J.; Jossang, T. *Phys. Rev. A* **1990**, *41*, 4199−4209.
(45) Fleer, G. J.; Stuart, M. A. C.; Scheutjens, J. M. H. M.; Crosgrove, T.; Vincent, B. *Polymers at Interfaces*; Chapman & Hall: London, 1993.
(46) Glynos, E.; Chremos, A.; Petekidis, G.; Camp, P. J.; Theofanidou, E.; Koutsos, V., manuscript in preparation.
(47) Rubinstein, M.; Colby, R. H. *Polymer Physics*; Oxford University Press: New York, 2003.
(48) Milner, S. T. *Science* **1991**, *251*, 905−914.
(49) Malescio, G.; Pellicane, G. *Nat. Mater.* **2003**, *2*, 97−100.
(50) Malescio, G.; Pellicane, G. *Phys. Rev. E* **2004**, *70*, 021202.
(51) Thiele, U.; Mertig, M.; Pompe, W. *Phys. Rev. Lett.* **1998**, *80*, 2869−2872.

MA0708803